Electronic structure and related thermal and magnetic properties of some ternary Invar alloys

B. Sanyal* and S. K. Bose†
Physics Department, Brock University, St. Catharines, Ontario, Canada L2S 3A1
(Received 18 May 2000)

We present first-principles electronic structure calculations of some face-centered-cubic disordered ternary Invar alloys, using the tight-binding linearized muffin-tin orbital method combined with the coherent-potential approximation (TB-LMTO-CPA). We calculate the total energies, equilibrium lattice parameters, bulk moduli, magnetic moments, and hyperfine fields for Fe-Ni-Co, Fe-Ni-Pd, and Fe-Ni-Pt Invar alloys. Charge densities at the nuclei, which can be used to interpret the results of isomer shift experiments in these alloys, are also presented. The effects of systematic Co, Pd, and Pt substitution in binary $Fe_{65}Ni_{35}$ alloy on the above properties are carefully examined. We examine the high moment to low moment transition by varying the concentration of Fe. Total-energy curves as a function of the lattice parameter show two distinct minima corresponding to the ferromagnetic (high moment and high volume) and nonmagnetic (zero moment and low volume) states. By using the Debye-Grüneisen model, we calculate thermal-expansion coefficients of these alloys near the Invar compositions. The results are in qualitative agreement with the experimental trend. Finally, we present results for the effective exchange coupling parameter in these alloys following the LMTO-CPA treatment of Liechtenstein *et al.* [J. Magn. Magn. Mater. **67**, 65 (1987)]. Comparison of the calculated quantities with available experimental results is provided, wherever appropriate and feasible.

I. INTRODUCTION

The study of the Invar effect in alloys has been an active field of research since its discovery by Guillaume[1] in 1897. The most typical Invar system is the random fcc $Fe_{65}Ni_{35}$ alloy, which shows almost zero thermal expansion over a wide temperature range around room temperature. The term ''Invar'' is thus used to describe solids exhibiting invariance of length (volume) with respect to temperature. Since the discovery of the Invar effect in random Fe-Ni alloys by Guillaume, a large number of alloys with Invar properties have been discovered, and several theoretical models have been proposed to explain the observed properties of these alloys. A common feature of these alloys is that they are close to (and on the magnetic side of) a ferromagnetic to nonmagnetic transition. The transition from a high volume ferromagnetic state to a low volume nonmagnetic state occurs in these alloys when the iron concentration is increased beyond its value in the Invar region. The difference between the energies of the magnetic and the nonmagnetic states immediately above and below the transition is very small, as verified by *ab initio* electronic structure calculations. This result and the proximity of the Invar alloys to the transition form the basis of the so-called 2γ-state model, originally put forward by Weiss[2] as an explanation of the Invar property. According to this model the Invar property is a consequence of the coexistence of high volume (magnetic) and low volume (nonmagnetic) states in the alloy. As the temperature is increased, thermal excitation of the nonmagnetic low volume states is supposed to offset the usual thermal expansion due to anharmonic lattice vibrations. A large body of experimental results as well as theoretical models and calculations pertaining to Invar alloys now exist. Interested readers are referred to the review articles by Shiga[3] and Wassermann.[4,5]

Recent theoretical studies of both ordered and disordered alloys have been done mainly by first-principles electronic structure calculations based on the fixed spin moment (FSM) method. Electronic structure calculations of ordered FeNi and FePt alloys were performed extensively by Podgórny[6] using the linear muffin-tin orbital (LMTO) method.[7] Fe_3Ni was also studied by Entel *et al.*[8] to show the connection between the Invar effects with martensitic transformations, magnetovolume instabilities, and the low moment–high moment transitions. They employed the augmented spherical wave method for zero-temperature calculations, combined with the spin-fluctuation theory for finite temperatures. Moroni *et al.*[11] have presented results of LMTO calculations for several ordered Fe-Ni compounds based on the standard floating-spin method where the magnetic moment is the result of the calculation for a fixed lattice parameter. The influence of atomic disorder on the structural and magnetic instabilities of random Fe_xNi_{1-x} alloys was studied by Abrikosov *et al.*[9], who calculated several ground-state properties for the whole concentration range using the LMTO-CPA method. Similar studies for random Fe_xNi_{1-x} alloys were carried by Schröter *et al.*[10] for concentrations near the Invar region using the Korringa-Kohn-Rostoker coherent-potential approximation (KKR-CPA) scheme. Recently Hayn and Drchal[12] calculated properties of disordered Fe_xPt_{1-x} alloys using the LMTO-CPA method. All these calculations involving disordered alloys employed the FSM scheme, and confirmed the existence of two local minima with different volumes near the Invar compositions. The binding-energy curves show two distinct branches with a small energy difference between their respective minima and thus the idea of the two-state model is qualitatively confirmed. The possibility of antiparallel spin alignments in these alloys has been considered in the KKR-CPA formulation[13] of the disordered local moment (DLM) model.[14] Using the locally self-consistent multiple scattering method, Wang *et al.*[15] have studied the noncollinear magnetic structure of the $Fe_{65}Ni_{35}$ alloy. They obtain evidence suggesting the coexistence of

ferromagnetism and antiferromagnetism in this alloy. In a recent work, Schilfgaarde *et al.*[16] have presented *ab initio* calculations that allow for noncollinear spin alignments, where the local spin direction can deviate from the direction of the average magnetic moment. According to their calculations, the magnetic structure is characterized by a continuous transition from the high spin (HS) state at high volumes to a disordered noncollinear low spin (LS) state at low volumes. This noncollinearity gives rise to an anomalous volume dependence of the binding energy, leading to many of the observed idiosyncrasies of Invar alloys.

Theoretical investigations of disordered Invar alloys have so far been restricted to binary systems only. To bridge this gap, we present results for disordered ternary alloys, fcc Fe-Ni-Co, Fe-Ni-Pd, and Fe-Ni-Pt, calculated using the tight-binding (TB)-LMTO-CPA method in the atomic-sphere approximation (ASA).[7] We calculate the properties of these alloys around the Invar compositions as well as through the ferromagnetic to nonmagnetic (FM-NM) transition. Two series of calculations are presented.

Case I: Keeping the concentration of Fe fixed at 65%, we vary the concentration of Ni by adding Co, Pd, and Pt. This shows the deviation of properties of $Fe_{65}Ni_{35}$ alloy as the third component is being added gradually.

Case II: Varying the concentration of Fe in each alloy we study the FM-NM transition and its effect on various physical properties.

In addition to calculating the standard cohesive, thermal, and magnetic properties, we have examined the exchange interaction in these alloys. An understanding of the nature of the exchange interactions in these alloys and their variation with respect to volume and composition, especially near the FM-NM transition, may shed new light on the nature of the Invar problem. In pure fcc Fe the transition from the high volume and high moment state to the low volume and zero moment state is accompanied by a rapid decrease in the exchange coupling constant,[17] which changes from a positive to a large negative value before rising back to zero as the system is compressed. Thus the system changes from ferromagnetic to antiferromagnetic and then to paramagnetic as a result of gradual compression. This strong magnetovolume effect is expected to be a common feature of all Invar alloys. To demonstrate this we study the variation of the exchange coupling constant in the ternary Invar systems by increasing the Fe concentration gradually beyond the FM-NM transition. We also provide results for the composition dependence of the average exchange coupling constants in some of the ternary Invar alloys for a fixed Fe concentration of 65%.

In the single-site approximation of the CPA, as used in this work, any chemical short-range order in the alloy is completely neglected. A certain degree of chemical short-range order is usually present in the disordered alloys at low temperatures. For magnetic solids the problem is further complicated by the fact that chemical short-range order and the magnetic state are interrelated. Admittedly the neglect of chemical short-range order introduces some error in the calculated properties of the alloys. However, experience from the application of the LMTO-ASA-CPA to binary transition-metal alloys suggests that, for the alloys considered, magnetic moments should agree to within 20% of the experimental results. Most of the difference will be due to the fluctuations in the near-neigbor environment of Fe, since among all the component metals considered Fe (in the fcc phase) exhibits the strongest magnetovolume effect and sensitivity to near-neighbor environment. Calculations of charge densities at the nuclei for ordered and disordered alloys of the same composition reveals only small differences between the ordered and the disordered states, provided both are magnetic or nonmagnetic. In view of this, it would be safe for us to claim that the trends in the variation of physical quantities with composition and lattice parameter presented in this paper should be reliable. The neglect of chemical short-range order should have a small effect on the exact locations and magnitudes of the discontinuities (sharp changes) in the various quantities at the FM-NM transition. It is important to note that in a noncollinear spin model treatment, similar to that of Wang *et al.*,[15] these discontinuities would appear somewhat smoother. The organization of this paper is as follows: in Sec. II we describe the method of calculation followed by the results of total-energy calculations in Sec. III. Section IV contains a discussion of our results followed by the conclusions.

II. METHOD OF CALCULATION (TB-LMTO-CPA)

The total-energy calculations were done using the TB-LMTO-CPA method for the disordered ternary alloys. Readers are referred to Ref. 18 for a detailed discussion of the method. Our calculations are based on the usual floating-spin moment scheme where the magnetic moment is the result of the calculation for a fixed lattice parameter. On the other hand, the fixed spin moment (FSM) calculation involves determining the total energy as a function of both magnetic moment and lattice parameter. As pointed out by Hayn and Drchal[12] the two approaches are equivalent in the sense that for a given lattice parameter the magnetic moment calculated by the standard floating-spin moment approach is the same as the magnetic moment for which the FSM total energy has its minimum. In practice, the floating-spin moment approach may run into some convergence problem in the region of the moment-volume instability.[9] We have tried to avoid the convergence problem by carefully monitoring the mixing of the initial and final charges during the iterations and increasing the number of **k** points. We have compared our results for Fe_xNi_{1-x} with those of Abrikosov *et al.*[9] Apart from the fact that our method yields the FM-NM transition at a slightly higher Fe concentration than obtained by these authors, the agreement is very good. For compositions near the Invar region the agreement is excellent. Thus the results presented are reliable, except for the possibility of a slight overestimation of the Fe concentration at which the transition takes place. Physical quantities related to compositions away from the transition, as well as the magnitudes of the discontinuities in various quantities at the transition, are accurate within the uncertainties of the approximations involved.

Ground-state properties were calculated for lattice parameters that correspond to the minimum of the total energy. The calculations are partially scalar-relativistic in the sense that although the wave functions are nonrelativistic, first order perturbation corrections to the energy eigenvalues due to the Darwin and the mass-velocity terms are included. **k** space integrations were usually performed over the irreducible

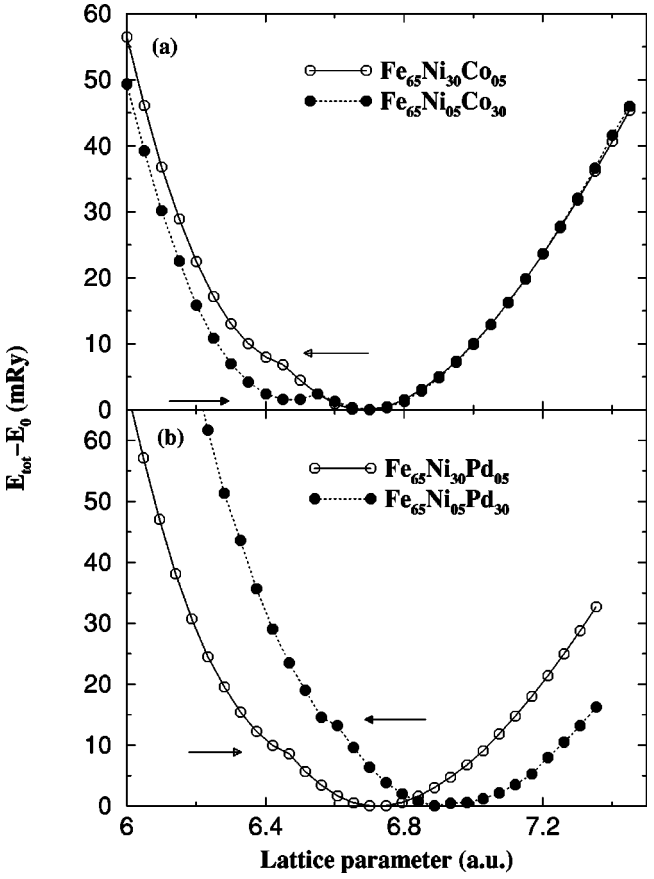

FIG. 1. Total energy vs lattice parameters for (a) Fe-Ni-Co and (b) Fe-Ni-Pd alloys. Bold lines with open circles show less Co content in (a) and less Pd content in (b). Dotted lines with filled circles show more Co content in (a) and more Pd content in (b). The arrows with open heads indicate the positions of minima of NM regions of the total-energy curves with less Co (Pd) content, while those with filled heads are for larger Co (Pd) content.

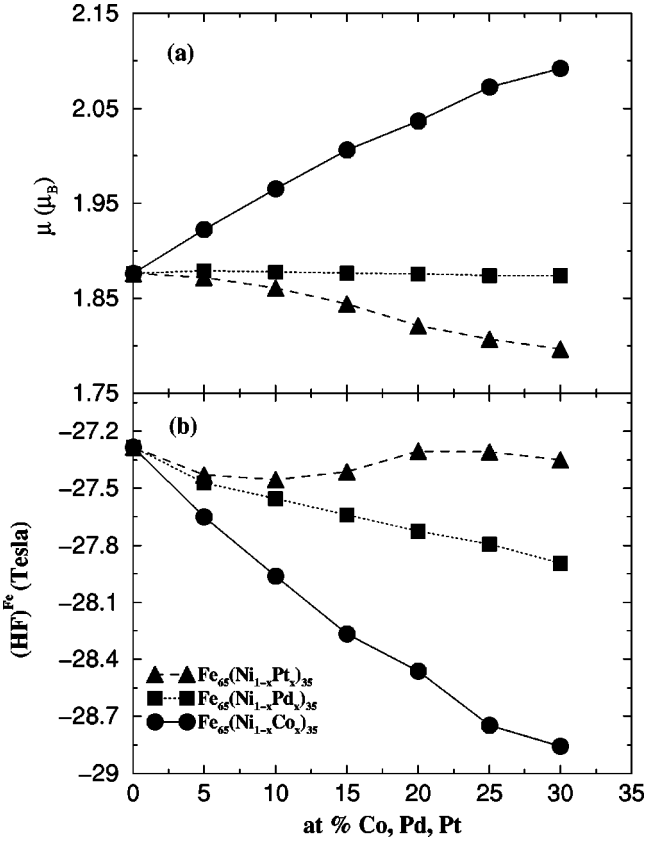

FIG. 2. Average magnetic moments of $Fe_{65}Ni_xX_{1-x}$ alloys in Bohr magnetons/atom (a) and hyperfine fields at Fe nuclei (b) with varying concentrations of X, where $X=$Co, Pd, and Pt.

wedge of the Brillouin zone using 280 **k** points. The number of **k** points was increased for calculations near the moment-volume instability. Energy integrations were performed using a semicircular contour in the complex energy plane for 12 points. The exchange correlation functional used is that of von Barth and Hedin.[19] In all the calculations, the lattice relaxation effects were included following the treatment suggested by Kudrnovský and Drchal.[18] To avoid having to compute the Madelung energy, the constituent spheres were made charge neutral (with charge transfer $\sim 1/10\,000$th of an electron). The choices of radii were made carefully to insure that the sphere-overlaps stay within the range of validity of atomic-sphere approximation (ASA). Total energy, local, and average magnetic moments, charge and spin densities at the nuclei are all usual products of the calculation.

A. Elastic and thermal properties

From the total-energy versus lattice parameter curves, we calculated the ground-state ($T=0$) bulk modulus (B) at zero pressure. Grüneisen parameter for low temperature (LT), γ_{LT}, was calculated by using the Debye-Grüneisen model as described by Moruzzi *et al.*:[20]

$$\gamma_{LT}=-1-\frac{V}{2}\frac{\partial^2 P/\partial V^2}{\partial P/\partial V}, \tag{1}$$

where P and V are pressure and volume, respectively. To obtain a qualitative variation of the thermal-expansion coefficient (α) with respect to Fe concentration we follow the approach used by Moruzzi *et al.*[20] Using the Debye-Grüneisen approximation, the free energy can be expressed as

$$F^{vib}(r,T)=E(r)+E_D^{vib}(r,T)-TS_D^{vib}(r,T), \tag{2}$$

where $E(r)$ is the total energy at 0 K for a Wigner-Seitz radius r. $E_D^{vib}(r,T)$ and $S_D^{vib}(r,T)$ are the thermal vibrational energy and vibrational entropy, respectively, at temperature T in the Debye model. They can be calculated from the standard expressions:

$$E_D^{vib}(r,T)=E_0+3k_BTD(\Theta_D/T)$$

$$S_D^{vib}(r,T)=3k_B\{4/3D(\Theta_D/T)-\ln[1-\exp(-\Theta_D/T)]\}, \tag{3}$$

where Θ_D is the Debye temperature. $E_0=9/8k_B\Theta_D$ is the zero-point energy and k_B is the Boltzmann constant. $D(\Theta_D/T)$ is the Debye function obtained from the tabulated values.[23] Finally, $\alpha(T)$ is calculated as

$$\alpha(T)=\frac{1}{r_0}\frac{dr_0}{dT}, \tag{4}$$

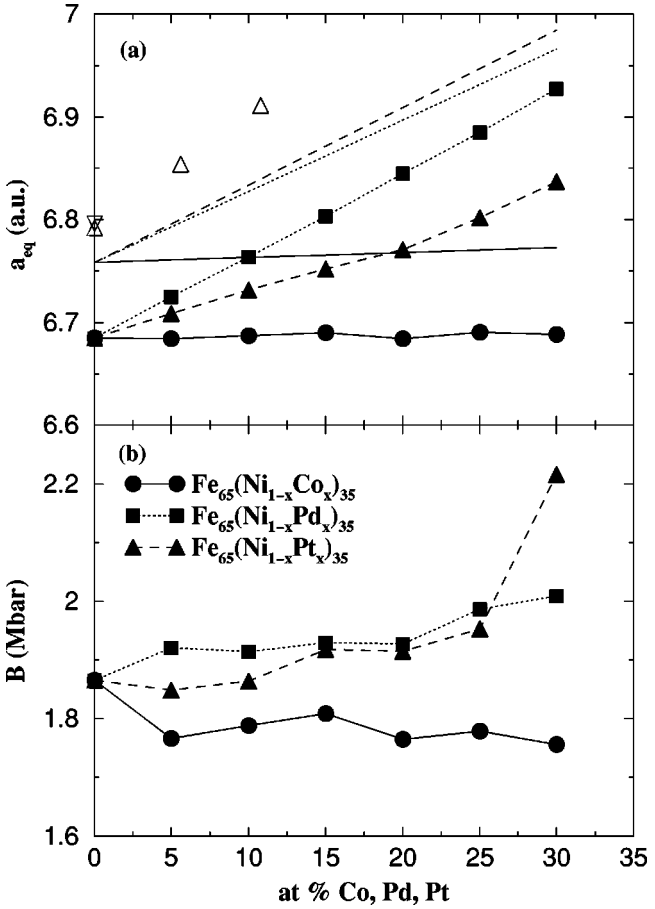

FIG. 3. (a) Equilibrium lattice parameters of $Fe_{65}(Ni_{1-x}X_x)_{35}$ alloys as a function of X, as described in Fig. 2. $Fe_{65}(Ni_{1-x}Co_x)_{35}$ (bold line with filled circles); $Fe_{65}(Ni_{1-x}Pd_x)_{35}$ (dotted line with filled squares); $Fe_{65}(Ni_{1-x}Pt_x)_{35}$ (dashed line with filled triangles). Bold, dotted, and dashed lines correspond to the Vegard's law values for $Fe_{65}(Ni_{1-x}Co_x)_{35}$, $Fe_{65}(Ni_{1-x}Pd_x)_{35}$, and $Fe_{65}(Ni_{1-x}Pt_x)_{35}$ alloys, respectively. The open triangles denote experimental values obtained from Ref. 22 and the inverted triangle is from Ref. 21. (b) Bulk moduli at equilibrium lattice parameters for the alloys.

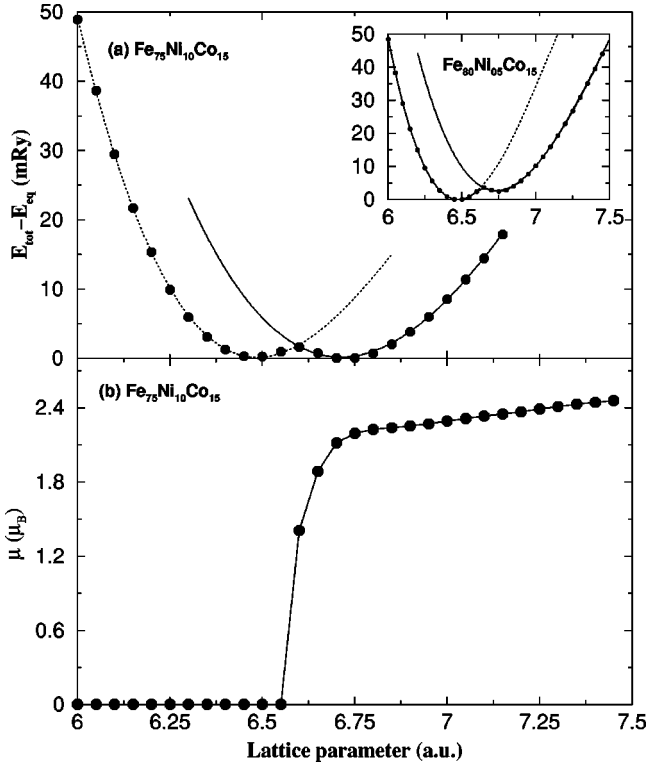

FIG. 4. (a) Total-energy vs lattice parameters for $Fe_{75}Ni_{10}Co_{15}$ and $Fe_{80}Ni_{05}Co_{15}$ (inset) alloys. Energies have been measured from ground-state energy taken as zero. The dotted and the bold curves are the fitted polynomials. (b) Average magnetic moment as a function of lattice parameters for $Fe_{75}Ni_{10}Co_{15}$ alloy.

where r_0 is the Wigner-Seitz radius corresponding to the minimum of the free-energy curve for a particular temperature T. Following the suggestion by Moruzzi *et al.*[20] we approximate Θ_D by $41.63(r_0B/M)^{1/2}$, where B and M are the bulk modulus and average atomic weight, respectively. This expression for Θ_D, as discussed by Moruzzi *et al.*,[20] should be valid for metallic systems with Poisson's ratio close to $\frac{1}{3}$. For Fe, Co, and Ni this ratio is close to 0.30 and for Pt it is 0.39. Hence the above expression for Θ_D should be valid for the alloys under study. As a check, we compare the values of Θ_D calculated this way with the values obtained from the concentration weighted average of the Debye temperatures of the pure elements.[21] The two approaches yield very similar values.

An alternative way of estimating the thermal-expansion coefficient is to use the well-known relation[22]

$$\alpha = \frac{\gamma_{LT} C_v}{3B}, \tag{5}$$

where C_v is the lattice specific heat at constant volume. For metals this expression should be modified to include the electronic contribution to the specific heat. As suggested by Ashcroft and Mermin,[22] for nearly-free-electron metals this expression can be modified to

$$\alpha = \frac{\left(\gamma_{LT} C_v + \frac{2}{3} C_{el}\right)}{3B}, \tag{6}$$

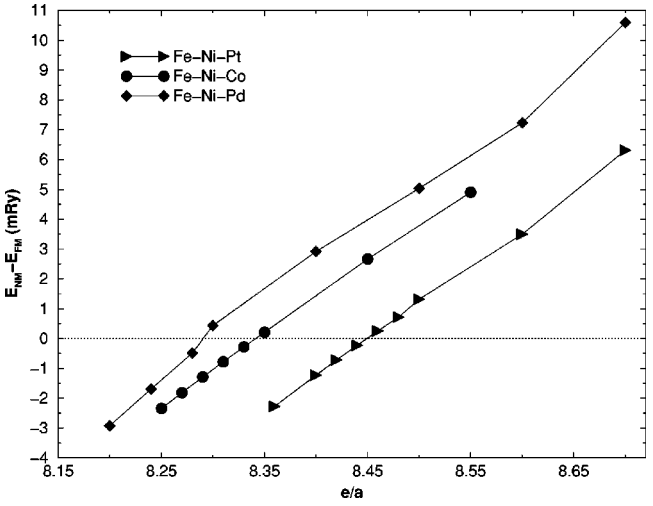

FIG. 5. Energy difference between the minima of nonmagnetic (NM) and ferromagnetic (FM) states as a function of electron per atom ratio (e/a) of the alloys. The dotted line shows the zero of energy difference. See text (discussion in the beginning of Sec. III B) for details of the exact compositions used in the calculations.

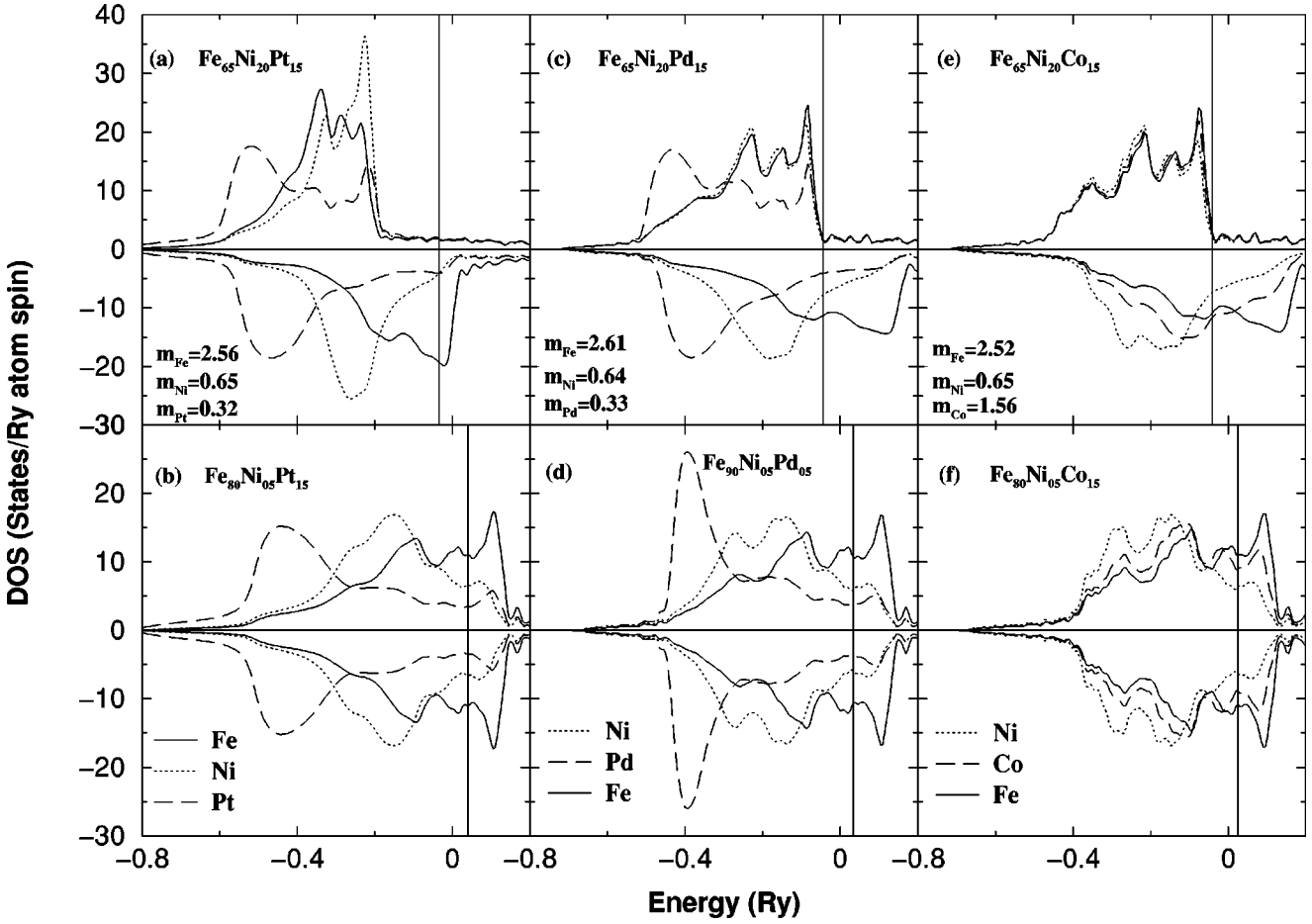

FIG. 6. Component-projected spin-resolved DOS. In all cases, the bold, dotted, and dashed lines are for Fe, Ni, and X partial DOS, where X=Co, Pd, and Pt. The vertical lines show the positions of the Fermi levels. The numbers in the upper panels (a, c, e) represent partial magnetic moments in Bohr magnetons/atom.

where C_{el} is the electronic specific heat. For metals with the Fermi level well within the d band the correction is harder to evaluate. However, for the thermal expansion at room temperature or even at the lowest temperatures at which α has been measured (around $-100\,^{\circ}\mathrm{C}$), the electronic contribution to specific heat is negligible compared to the contribution from lattice vibrations. Thus we use Eq. (5) to (second) estimate α from the calculated values of γ_{LT}, B, and from the tabulated values[23] of the Debye model expression for the lattice specific heat. Note that Eq. (5) is commonly used for evaluating the Grüneisen parameter from calculated values of the bulk modulus, specific heat, and the thermal-expansion coefficient.[24]

B. Exchange interactions

We calculate the total exchange coupling parameter J_o as a function of concentration following the prescription of Liechtenstein *et al.*[25,26] Essentially, the method is based on mapping the change in energy due to the deviation of a single spin, at a reference site o, from the collinear ferromagnetic ground state onto an effective Heisenberg model. The change in energy corresponding to this small spin-density perturbation is approximated by the change in the sum of one-electron energies by appealing to Andersen's ''local force theorem.''[27] Using Lloyd's formula[28] one can express the sum of one-electron energies in terms of the scattering-path operator or the auxiliary Green's function. In LMTO the latter can be evaluated from a knowledge of the potential function and the structure constant matrix. Mapping the change in energy onto a Heisenberg model results in an expression for the exchange coupling constant:

$$J_o=\sum_j J_{oj}, \tag{7}$$

the sum of the exchange interactions between the reference spin and all its neighbors. In a mean-field theory this coupling constant is proportional to the Curie temperature T_C of the system. For a multicomponent random alloy the mean-field estimate of T_C can be assumed to be proportional to the concentration weighted average of the coupling constants calculated for the component atoms. Thus for the random ternary alloys we calculate the average coupling constant as

$$J_o=x_AJ_A+x_BJ_B+x_CJ_C, \tag{8}$$

where J_i's ($i=A/B/C$) are the exchange coupling constants for atoms A,B, and C considered as impurities in the effective CPA medium and x_i's are the concentrations of the individual components. J_i is given by the following expression:

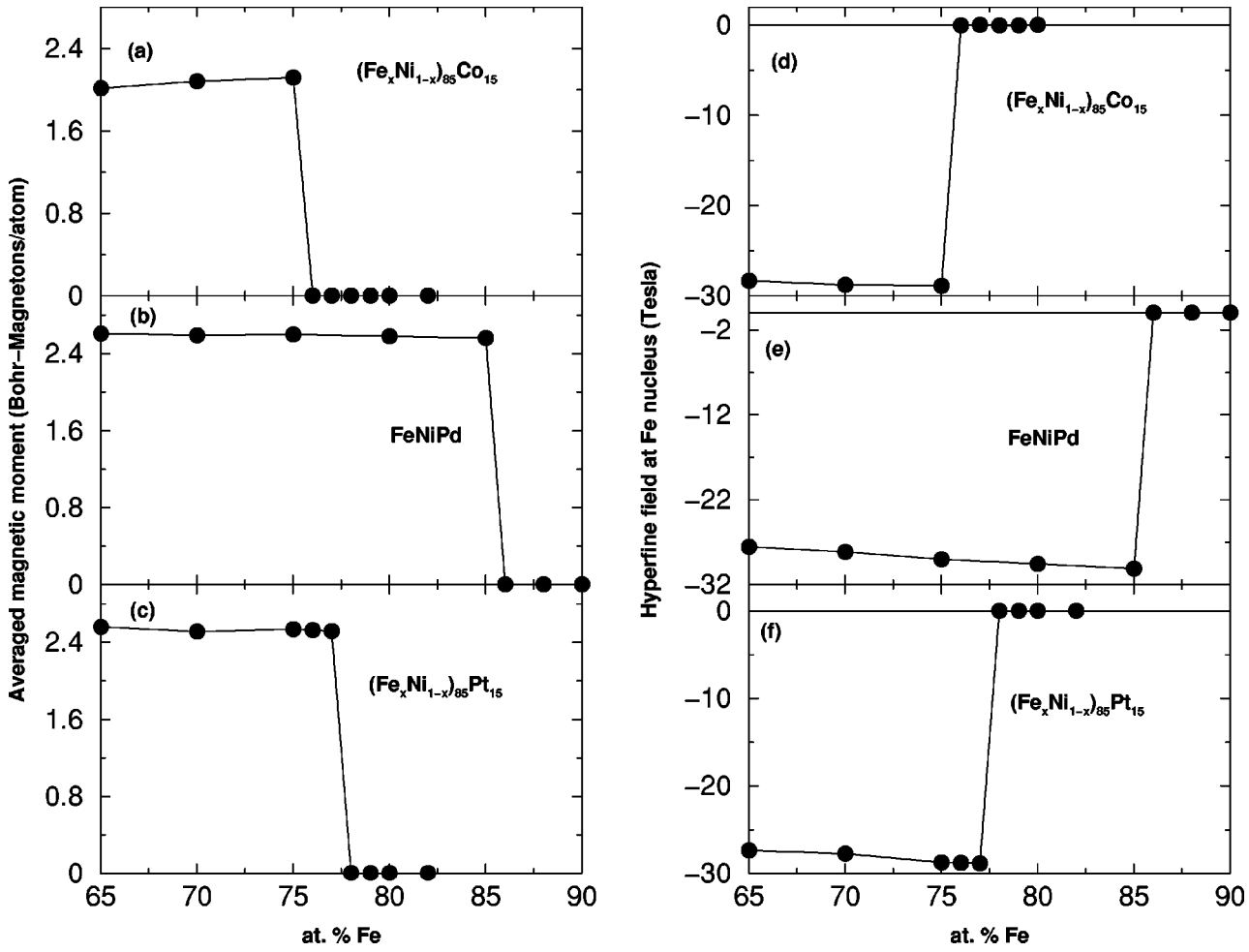

FIG. 7. (a)–(c): Average magnetic moments as a function of Fe concentration for (a) $(Fe_xNi_{1-x})_{85}Co_{15}$; (b) $(Fe_xNi_{1-x})_{85}Pd_{15}$ (after 85% of Fe, the three plotted points are for $Fe_{86}Ni_{07}Pd_{07}$, $Fe_{88}Ni_{06}Pd_{06}$, and $Fe_{90}Ni_{05}Pd_{05}$); (c) $(Fe_xNi_{1-x})_{85}Pt_{15}$. (d)–(f): Hyperfine fields at Fe nuclei as a function of Fe concentration for the same compositions described above.

$$J_i = -\frac{1}{4\pi}\sum_L \int^{E_F} dE\ \mathrm{Im}\{\Delta_L^i(z)[T_{L\uparrow}^i(z) - T_{L\downarrow}^i(z)] + \Delta_L^i(z)T_{L\uparrow}^i(z)\Delta_L^i(z)T_{L\downarrow}^i(z)\}, \tag{9}$$

with

$$\Delta_L^i(z) = \mathcal{P}_{L\uparrow}^i(z) - \mathcal{P}_{L\downarrow}^i(z),$$

$$\mathcal{P}_{L\sigma}^i(z) = [z - C_{L\sigma}^i][\Delta_{L\sigma}^i + \gamma_{L\sigma}^i(z - C_{L\sigma}^i)]^{-1},$$

$$T_{L\sigma}^i(z) = \langle g_{L\sigma}^\beta(z)\rangle\{1 + [\mathcal{P}_{L\sigma}^i(z) - \tilde{\mathcal{P}}_{L\sigma}(z)]\langle g_{L\sigma}^\beta(z)\rangle\}, \tag{10}$$

where σ is the spin index ($\uparrow$ or $\downarrow$). $\mathcal{P}_{L\sigma}^i$ is the potential function of the component i for orbital L and spin σ. The potential function has been expressed above in terms of the potential parameters C, Δ, and γ of the LMTO Hamiltonian. z is the complex energy and E_F is the Fermi energy of the alloy, $\langle g_{L\sigma}^\beta(z)\rangle$ is the configuration averaged auxiliary Green function within the CPA and $\tilde{\mathcal{P}}$ is the coherent-potential of the medium. The CPA calculation is performed by invoking the usual single-site approximation.

III. RESULTS AND DISCUSSION

A. Case I

Our motivation for this part is to explore the effects of gradual addition of a third component from $3d$, $4d$, and $5d$ series to $Fe_{65}Ni_{35}$ alloy. We have chosen Co($3d$), Pd($4d$), and Pt($5d$) to be the third component to be added. For all cases, the concentration of Fe has been fixed to be at 65%. The addition of Pd or Pt does not change the electron per atom (e/a) ratio from its value of 8.7 for the $Fe_{65}Ni_{35}$ alloy. With the addition of Co this ratio is reduced below 8.7. The results are presented in Figs. 1(a) for Fe-Ni-Co and 1(b) for Fe-Ni-Pd. In all cases, the resulting total-energy curves show two minima, one with a large magnetic moment and a large lattice parameter and the other with a smaller lattice parameter and with zero magnetic moment. The energy difference between the two minima decreases with the addition of Co, and increases with the addition of Pd and Pt (not shown in the graph). Thus the transition from the ferromagnetic to nonmagnetic state becomes easier (harder) with the addition of Co (Pd, Pt). The reduction of e/a ratio from 8.7 (0% Co) to 8.4 (30% Co) drives the system towards a region of strong magnetovolume instability in the case of Co-substituted $Fe_{65}Ni_{35}$ alloy. For Pd- and Pt-substituted ternary alloys, the

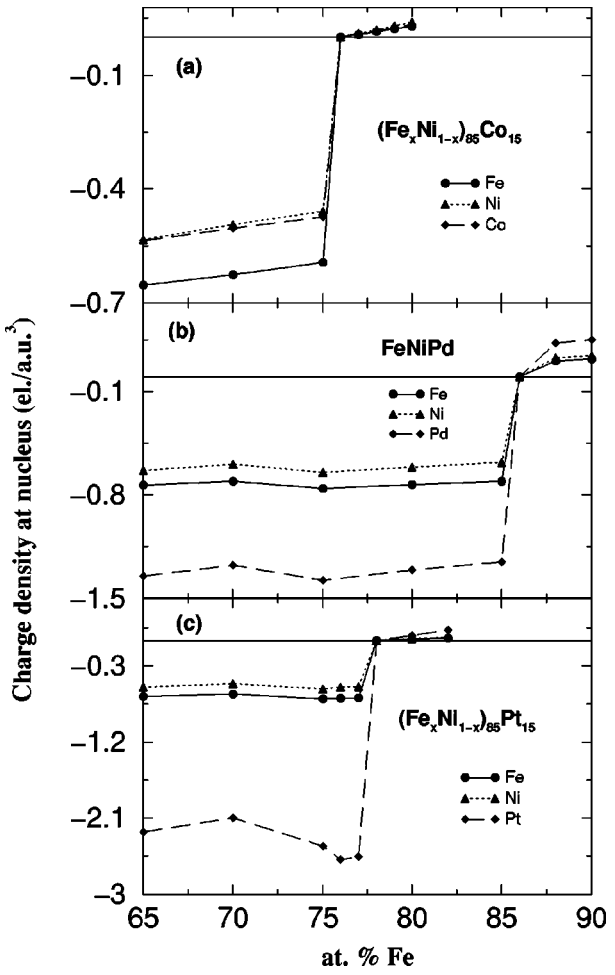

FIG. 8. Total (core+valence) charge densities at component nuclei. The charge densities are shown relative to their values at (a) 76%, (b) 86%, and (c) 78% of Fe in the alloys. The bold horizontal lines show the positions of zero charge differences. See text (discussion in the beginning of Sec. III B, and the caption of Fig. 7) for the details of the exact compositions used in the calculations.

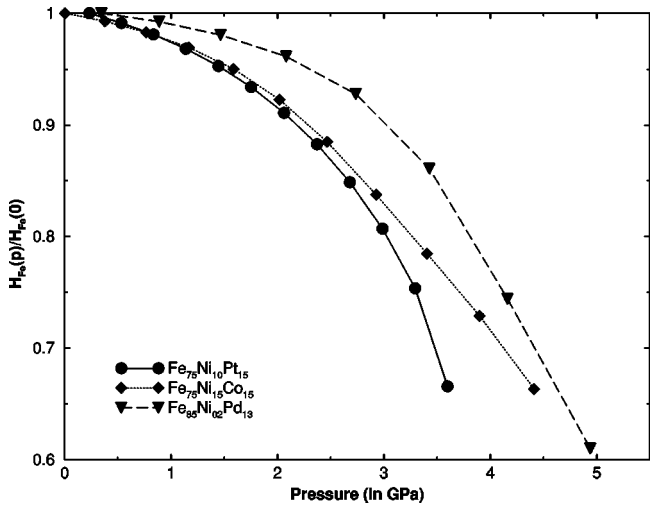

FIG. 9. Ratio of hyperfine fields at Fe nuclei at nonzero and zero pressure (equilibrium) as a function of pressure for $Fe_{75}Ni_{10}Pt_{15}$ (bold line with open circles); $Fe_{75}Ni_{15}Co_{15}$ (dotted line with filled diamonds); $Fe_{85}Ni_{02}Pd_{13}$ (dashed line with filled triangles). The compositions selected are immediately on the magnetic side of the transition.

energy barriers (difference between the two minima) are larger than those found in binary $Fe_{65}Ni_{35}$ alloy. This is consistent with the known results[12] for binary alloys, where the barrier heights for $Fe_{75}Pt_{25}$ and $Fe_{70}Ni_{30}$ are quoted as 2.1 and 1.1 mRyd, respectively. Effects on magnetic properties are presented in Fig. 2. Figure 2(a) shows that the average magnetic moment increases with the gradual substitution with Co whereas the moments in Pd- and Pt-substituted alloys decrease. Change in moments in Pt alloys is more pronounced than in the Pd alloys, where the change is almost negligible. Partial magnetic moments at Fe sites increase in Pd- and Pt-substituted alloys, and decrease in Co-substituted alloys. But as Co is a magnetic substance, the average magnetic moments enhance as a result of substituting with Co. These changes are reflected in the changes in hyperfine field at the Fe nucleus [see Fig. 2(b)]. Our calculation of the hyperfine field at the Fe nucleus is restricted to the Fermi contact term with the core contribution set proportional to the local Fe magnetic moment, and follows exactly the prescription of Turek.[29] Hyperfine field values increase sharply in magnitude with the addition of Co. The changes for Pd- and Pt-substituted alloys are less pronounced, though the values of the hyperfine field are somewhat increased from the values for the $Fe_{65}Ni_{35}$ alloy.

Equilibrium lattice parameters and bulk moduli are presented in Fig. 3. Figure 3(a) shows that Co substitution hardly changes the equilibrium lattice parameter value of $Fe_{65}Ni_{35}$. This is expected as the Wigner-Seitz radii of Fe, Co, and Ni are similar. Addition of Pd or Pt increases the equilibrium lattice parameters due to their larger sizes. For comparison, we have also plotted the values of lattice parameters based on Vegard's law. There is a negative deviation from the Vegard's law values in all cases. For $Fe_{65}Ni_{35}$, the calculated value of the equilibrium lattice parameter is close to the value obtained by Abrikosov *et al.*,[9] but less than the experimental value of 6.796 a.u.[30] The experimental lattice parameters for Pt-substituted $Fe_{65}Ni_{35}$ alloy[31] for 5.6 and 10.8% Pt are also shown in Fig. 3(a). The deviation from experimental results is $\sim 3\%$. This underestimation of the lattice parameter in our calculation is partly due to the local spin-density approximation and partly due to the atomic-

TABLE I. Pressure effects on magnetic moment. Values of $(1/\tilde{\mu})(d\tilde{\mu}/dP)\times 10^{-12}$/Pa for different alloys. For each alloy system within the vertical bars, the first value is for a composition away from the FM-NM transition, while the second one is for a composition just before the transition.

	$Fe_{65}Ni_{20}Co_{15}$	$Fe_{75}Ni_{10}Co_{15}$	$Fe_{65}Ni_{20}Pd_{15}$	$Fe_{85}Ni_{02}Pd_{13}$	$Fe_{65}Ni_{20}Pt_{15}$	$Fe_{77}Ni_{08}Pt_{15}$
$\frac{1}{\tilde{\mu}}\frac{d\tilde{\mu}}{dP}$	-8	-23	-7	-27	-11	-33

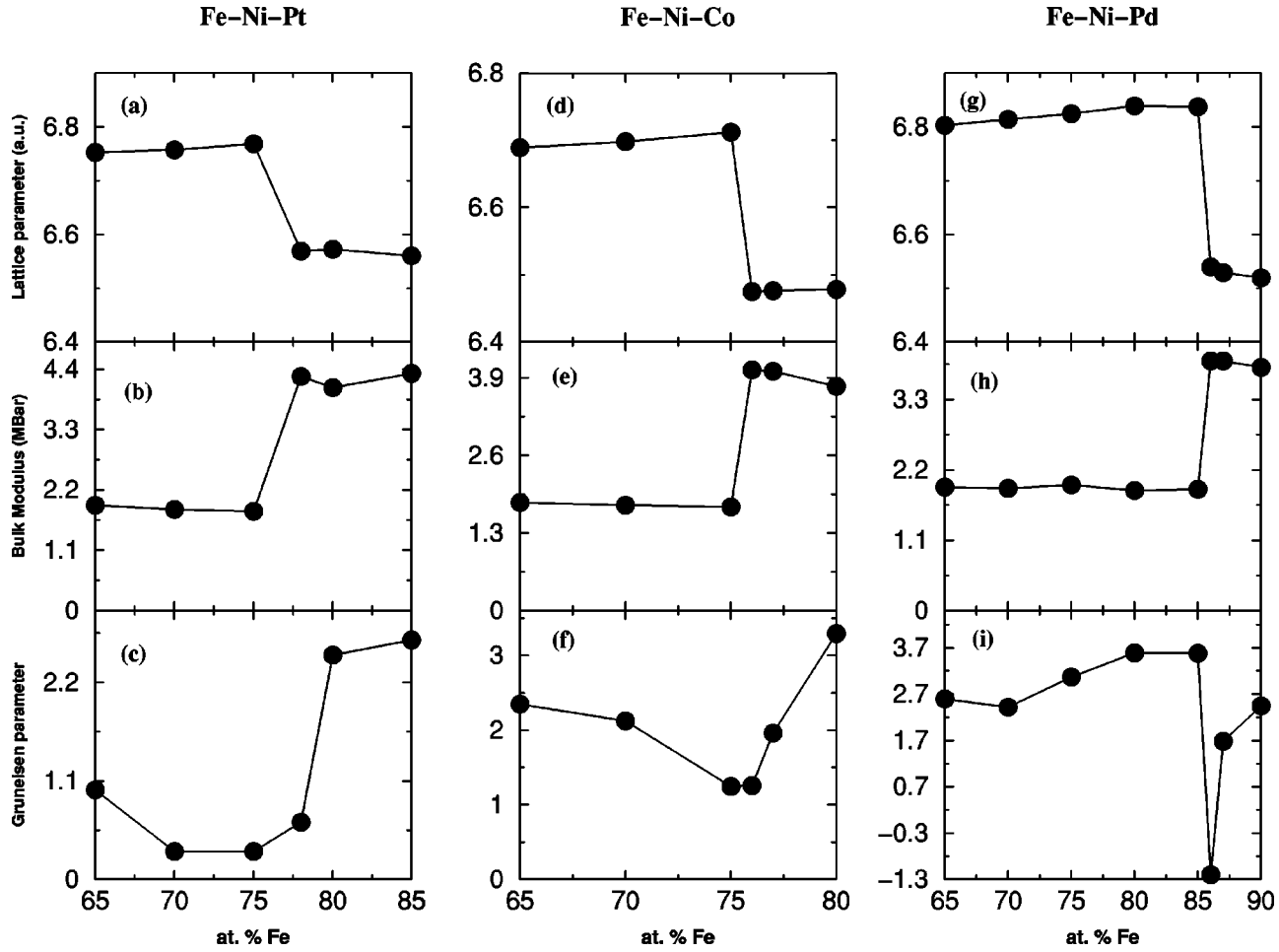

FIG. 10. Equilibrium lattice parameters, bulk moduli, and Grüneisen parameters as a function of Fe concentration for Fe-Ni-Pt (a)–(c), Fe-Ni-Co (d)–(f), and Fe-Ni-Pd (g)–(i) alloys. See text (discussion in the beginning of Sec. III B, and the caption of Fig. 7) for details of the exact compositions used in the calculations.

sphere approximation (ASA) which resorts to making the charge-density spherically symmetric. These approximations also lead to an overestimation of the bulk moduli. Figure 3(b) shows that the bulk moduli values increase with the addition of Pd and Pt, and decrease with the addition of Co. For $Fe_{65}Ni_{35}$, we obtain a value of 1.87 MBar, less than that (~ 2 MBar) presented in Ref. 9, but greater than the experimental value: 1.06 MBar.[32] The expression $41.63(r_0 B/M)^{1/2}$ for the Debye temperature Θ_D, as suggested by Moruzzi *et al.*,[20] yields the values 381 and 347 K for $Fe_{65}Ni_{35}$ and $Fe_{65}Ni_{25}Pt_{10}$, respectively. These compare well with the values 385 K (0% Pt) and 300 K (10.8% Pt), quoted in Ref. 31.

B. Case II

In this case we vary the concentration of Fe in order to examine the FM-NM transition. This transition manifests itself in the form of sharp (almost discontinuous) changes in magnetic, cohesive (elastic) and thermal properties of the system. Calculation for Fe-Ni-Co and Fe-Ni-Pt systems were usually done by keeping the Co and Pt concentrations fixed at 15%, while the concentrations in the Fe-Ni matrix were varied through the FM-NM transition. This means that for these systems the transition could be achieved for 15% of Co or Pt. For $(Fe_xNi_{1-x})_{85}Co_{15}$ the transition was observed between 75% (magnetic) and 76% (nonmagnetic) of Fe. For $(Fe_xNi_{1-x})_{85}Pt_{15}$ the transition was found to be between 77% (magnetic) and 78% (nonmagnetic). For the Fe-Ni-Pd system the Fe concentration needed to be increased beyond 85% to obtain the transition, i.e., the Pd concentration needed to be lowered below 15%. Thus for this system calculations were performed for the formula unit $(Fe_xNi_{1-x})_{85}Pd_{15}$ for the total Fe concentration of 85% or less and then three compositions were selected: $Fe_{86}Ni_{07}Pd_{07}$, $Fe_{88}Ni_{06}Pd_{06}$, and $Fe_{90}Ni_{05}Pd_{05}$. A couple of comments are in order at this stage. First, as stated earlier, our floating-spin moment calculation overestimates slightly the Fe concentration at which the FM-NM transition takes place. Thus experimentally the transition is likely to be obtained at a Fe concentration lower than that suggested in this paper. Second, the changes in the physical quantities associated with the transition should be smoother (i.e., take place over a wider composition range) than what is given by our collinear magnetic model calculation, where the spin has only two degrees of freedom. As shown by van Schilfgaarde *et al.*,[16] in a noncollinear magnetic model, where the magnetic moment can vary locally in directions, these changes take place continuously as a function of composition. We divide the discussion of the calculated quantities into three different parts and provide a comparison with experimental results, as available.

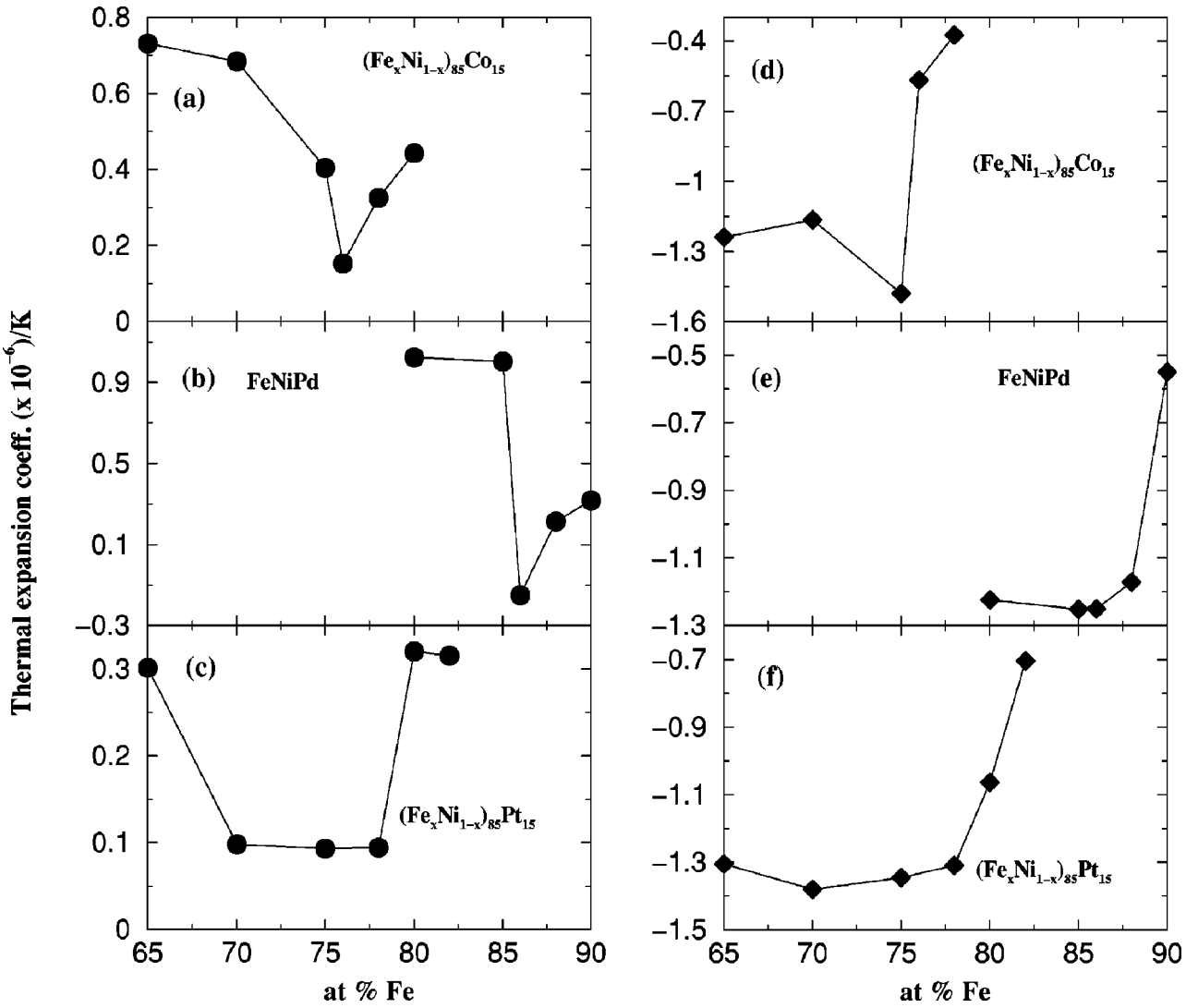

FIG. 11. Thermal-expansion coefficients vs concentrations of Fe for Fe-Ni-Co (a) and (d), Fe-Ni-Pd (b) and (e) and Fe-Ni-Pt (c) and (f) alloys. The right panel shows the results obtained by using Eq. (5), and the left panel shows the results from the minimization of free energy with the lattice vibrational contribution based on the Debye-Grüneisen model. See text (discussion in the beginning of Sec. III B, and the caption of Fig. 7) for details of the exact compositions used in the calculations.

1. Magnetic and related properties

In Fig. 4(a), we show the positions of the two energy minima in the case of Fe-Ni-Co alloys as functions of lattice parameter. For 75% Fe, the two minima are almost degenerate. Figure 4(b) shows the average magnetic moment with variation in volume of the system for this alloy. Up to this concentration the ground state of the system is ferromagnetic with a higher volume. The inset shows the same after the transition when the system becomes para(non)magnetic with a lower volume. Thus the nature of the magnetovolume instability is similar to that in other binary Invar alloys. These transitions are seen in Fe-Ni-Pd and Fe-Ni-Pt alloys as well at their respective critical concentrations of Fe. The critical concentrations of Fe at which the three systems become para(non)magnetic are 0.76, 0.86, and 0.78 for Fe-Ni-Co, Fe-Ni-Pd, and Fe-Ni-Pt, respectively. Approaching these critical concentrations, the energy difference between the two minima (FM and NM) decreases gradually. This is shown in Fig. 5. Addition of Fe reduces the electron/atom (e/a) ratio. The plot shows the variation of energy difference between the minima as a function of the e/a ratio of the alloy system. According to Fig. 3 of the review article by Wassermann,[4] alloys with an e/a between 8.5 and 9 are stable ferromagnets. In the range $8.5 \leqslant$ e/a $\leqslant 8.7$, the energy difference is still positive but the alloys show large magnetovolume instabilities. It is to be noted that $Fe_{65}Ni_{35}$ has an e/a value of 8.7. Further reduction of the e/a ratio leads to larger instabilities and the systems undergo a structural phase transition from the fcc phase to the bcc phase. In all of our calculations we have considered the alloys to be based on the fcc structure. We find that the transitions occur for e/a ratios between 8.3 and 8.45.

Figure 6 shows the component projected-spin-resolved densities of states for different alloy compositions in the FM and NM (nonmagnetic or paramagnetic) states along with the magnetic moments of individual components. The upper panel [Figs. 6(a), 6(c), and 6(e)] is for the FM states and the lower panel [Figs. 6(b), 6(d), and 6(f)] is for the NM states. For Pd- and Pt-substituted alloys, the peaks related to Pd or Pt are below the Fe and Ni peaks. From Fig. 6(e), it is seen

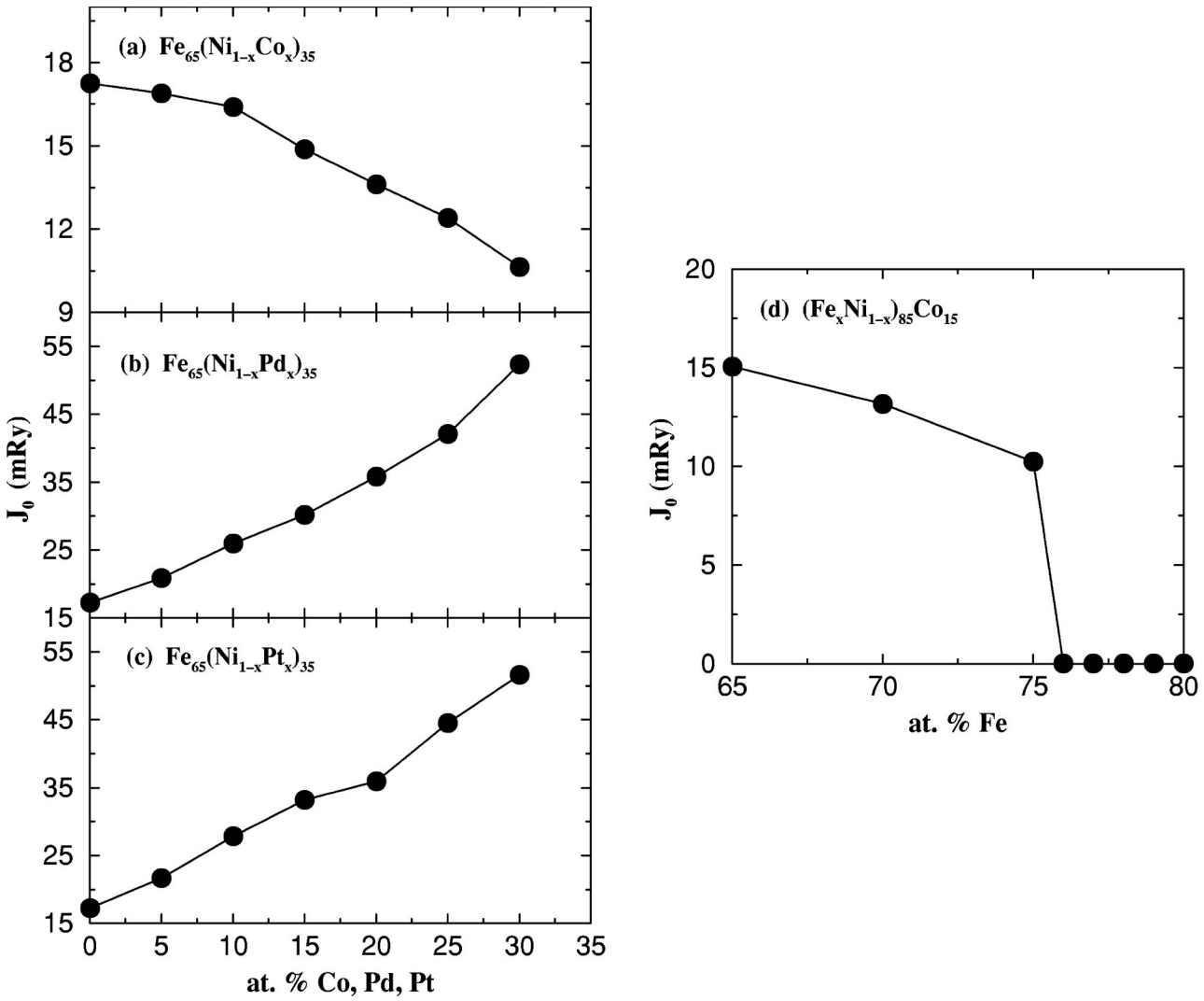

FIG. 12. Concentration-averaged exchange coupling constants for (a) $Fe_{65}(Ni_{1-x}Co_x)_{35}$, (b) $Fe_{65}(Ni_{1-x}Pd_x)_{35}$, and (c) $Fe_{65}(Ni_{1-x}Pt_x)_{35}$ alloys as a function of Co/Pd/Pt concentration. (d) represents the same for $(Fe_xNi_{1-x})_{85}Co_{15}$ alloy as a function of Fe concentration.

that the partial density of states (DOS) for majority spins are almost identical for Fe, Co, and Ni while the minority-spin DOS are shifted relative to one another. Exchange splitting of Fe majority and minority DOS is the highest among the three, and that for Ni is the lowest. This is manifested in the values of the magnetic moments. From (c), it is seen that the Fe moment is slightly higher in Pd-substituted alloy, while the Ni moments stay very similar in all the alloys. Note that Pt and Pd, on the verge of magnetic instability in the pure state, acquire magnetic moments in the alloy due to the presence of magnetic neighbors Fe and Ni. Pure Co is itself ferromagnetic and in the alloy its magnetism is somewhat diminished with respect to its pure state. The lowering of the lattice parameter in the para(non)magnetic state causes the bands to broaden, with a corresponding broadening of the peaks in the DOS and an overall lowering of the DOS everywhere.

Figure 7 shows the variation of magnetic properties with Fe concentration. Almost discontinuous changes in average magnetic moments and hyperfine fields at the Fe nuclei appear at the critical concentrations of Fe. The variations of magnetic moment and hyperfine fields in the FM region are almost linear with concentration. In Fig. 8 we present the charge density at component nuclei as a function of Fe concentration. The zero of the charge density has been taken to be that at the critical concentrations of Fe quoted above. At the FM-NM transition a sharp change in the charge density at the nuclei is expected, since the disappearance of the magnetic moment should accompany a transfer of charge from *d*- to *s*-like states. Thus, as the system passes from magnetic to nonmagnetic state, the charge density at the nuclei, which is due to *s* states only, should increase. Such a change should result in a noticeable change in isomer shift and should be observable experimentally. Recent ^{57}Fe Mössbauer isomer shift measurements in Fe-Ni fcc random alloys show a discontinuity of ~ 0.4 el/a_0^3 at the transition spanning a concentration range ~ 60–80 at. % Fe.[33] The values of charge densities are close for Fe, Ni, and Co nuclei, and are larger for Pd and Pt, as expected. Note that our charge-density calculation involves nonrelativistic wave functions, which are finite at the origin ($r=0$). The charge densities indicated at the nuclei are actually the charge densities at $r=0$. Since the first-order corrections to the energy due to Darwin and mass-velocity terms are included, this charge density comes out somewhat intermediate between those given by nonrelativis-

tic and scalar-relativistic calculations. The charge densities we report have a weak dependence on the sphere radii chosen for the component atoms. The latter were varied to keep the spheres charge neutral. Although this makes us avoid the problem of having to calculate the Madelung potential, the error due to the ASA changes with a change in sphere radii. Note that unlike standard LMTO calculations for crystalline solids, no combined correction terms are included in our calculations to reduce the ASA-related errors. In addition, the use of nonrelativistic wave function makes the charge densities for the alloys containing Pt less reliable.

In Fig. 9, we plot the ratio of hyperfine fields at the Fe nuclei at finite (nonzero) and zero pressures as a function of pressure. The ratio decreases from one at the zero pressure (equilibrium) to zero at a pressure around 4–5.5 GPa. Here the graph is shown up to the pressure where the ground state is ferromagnetic. This can be compared with the experimental results provided in Fig. 54(a) of the review article by Wassermann.[5] Though the experimental values are for the Fe-Ni and Fe-Pt binary alloys around the Invar composition, the general trend is similar to our results for the ternary systems. We also calculated pressure effects on magnetization. It is well known that near the Invar composition the logarithmic derivative of the magnetization M with respect to pressure P, $(1/M)(dM/dP)$, has a large negative value. We approximate this quantity by $(1/\tilde{\mu})(d\tilde{\mu}/dP)$ where $\tilde{\mu}$ is the average magnetic moment of the alloy. The results are presented in Table I. In all cases the values are quite high near the transition compared to those away from the transition. For comparison, the value of $(1/M)(dM/dP)$ for 33.6 at. % Ni in FeNi alloy is -80×10^{-12}/Pa, as obtained experimentally by Ono *et al.*[34]

2. Thermal and elastic properties

Ground-state properties such as equilibrium lattice parameters, bulk moduli, and Grüneisen parameters are plotted in Fig. 10 as a function of Fe concentration. All of these properties show anomalies around the critical (FM-NM) regions. These properties have been obtained at the equilibrium lattice parameters. Both the equilibrium lattice parameters and bulk moduli are almost linear functions of the Fe concentrations. As seen from the figures, the values of the Grüneisen parameters are highly anomalous at the region of transition. The values drop down at these regions and usually increase after the transition in the para(non)magnetic state. In the case of Fe-Ni-Pd, we even found a negative value for the Grüneisen parameter.

Figure 11 shows the calculated thermal-expansion coefficients as a function of Fe concentration. The left panel [(a)–(c)] shows the values calculated by using Eq. (5), while the right panel [(d)–(f)] shows the values obtained from free-energy minimization using the Debye-Grüneisen model, as discussed in Sec. II. A local minimum appears close to the composition where the FM-NM transition takes place. This kind of valley structure is qualitatively similar to what is observed experimentally in most of the Invar alloys. For example, Fig. 10-1 of the review article by Shiga[3] shows the thermal-expansion coefficients for FeNi alloys. We find the order of magnitude to be the same as in other binary Invar alloys. In spite of numerous approximations involved in estimating the thermal expansion coefficients, the results reproduce the correct trend and even yield negative expansion coefficients. For the sake of comparison with the experimental results of Fig. 10-1 of the review article by Shiga,[3] we used a temperature of $-100\,^{\circ}\mathrm{C}$ for calculating the expansion coefficients shown in Fig. 11. Note that a negative expansion coefficient can result from Eq. (5) only when the Grüneisen constant is negative.

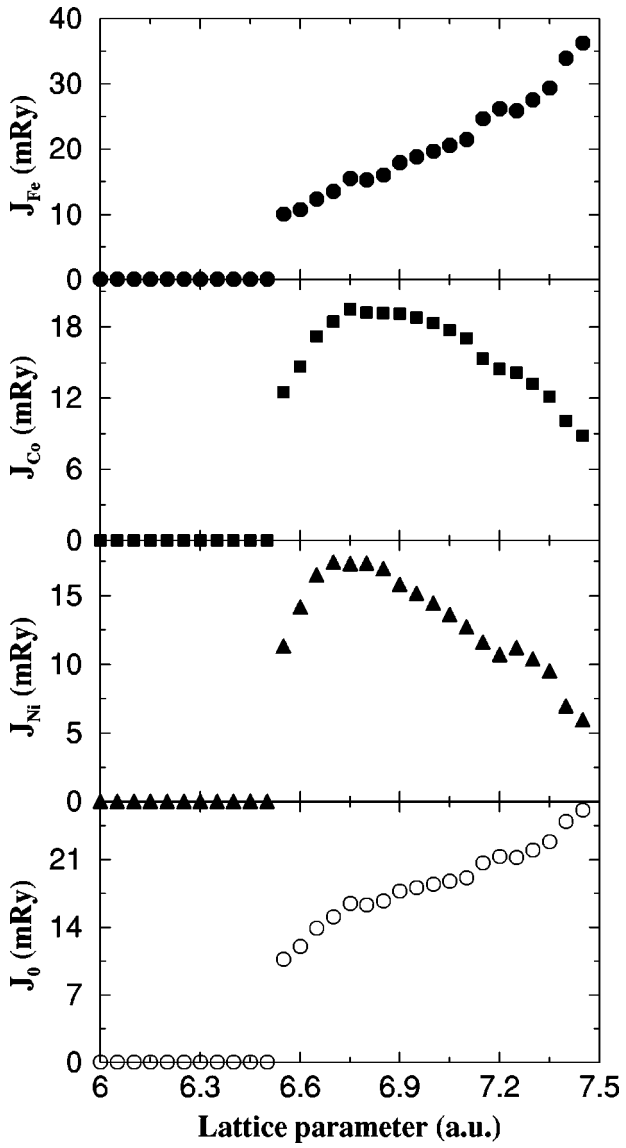

FIG. 13. Variation of the exchange coupling constant with lattice parameter in $Fe_{65}Ni_{20}Co_{15}$. The concentration averaged value and the values for the component atoms in the single-site CPA medium are shown.

3. Exchange interaction

Finally, we present the results of the calculations of the total exchange interaction parameters J_o. As a test case, we calculate the exchange parameter and hence the Curie temperature T_C ($T_C \propto J_o$) of pure bcc Fe and fcc Ni, using the relation $T_C = 2J_o/3k_B$. The calculated J_o's for Fe and Ni are 13 and 2.1 mRy, respectively. These yield Curie temperatures of 1430 K for bcc Fe and 225 K for fcc Ni which are comparable to the values of 1260 and 225 K obtained by Staunton *et al.*[35] The use of the CPA for the alloy phase and

the above mean-field expression relating the Curie temperature to J_o both overestimate T_C. Note also that T_C is overestimated in a Stoner-like theory where the transition from a ferromagnetic to a para(non)magnetic state results from a complete disappearance of local moments. It is expected that a noncollinear description of itinerant magnetism would reduce T_C. Our estimate of T_C for $Fe_{65}Ni_{35}$, 1800 K, is thus understandably higher than the experimental value of 505 K.[3]

Except for an overestimation of the exchange coupling constant, our calculation is able to produce the correct trend. Figures 12(a)–12(c) shows the values of J_o as a function of varying concentrations of Co, Pd, or Pt for the alloys mentioned in Case I. J_o decreases with an increase in Co concentration, and increases with the addition of Pd or Pt. Figure 12(d) shows the dependence of J_o as a function of Fe concentration for $(Fe_xNi_{1-x})_{85}Co_{15}$ alloys. With increase in Fe concentration, J_o decreases and becomes zero at the critical concentration. Thus, the disappearance of the average local moment is accompanied by disappearance of the average exchange interaction, a result related to the strong magnetovolume effect of fcc Fe. This magnetovolume effect in the exchange interaction of fcc Fe is believed to be the key element of all Invar alloys. There are suggestions that in Fe-Ni Invar alloys the frustration resulting from nearest-neighbor Fe-Fe antiferromagnetic exchange and ferromagnetic Fe-Ni and Ni-Ni exchange together with a rapid change with distance in the Fe-Fe exchange interaction are a prerequisite to conditions leading to the Invar properties.[36–38] The strong volume dependence of the exchange coupling seen in fcc Fe (Ref. 17) is retained in the alloy phase. Figure 13 shows the variation of the exchange coupling constant in $Fe_{65}Ni_{20}Co_{15}$ with the lattice parameter. The exchange coupling constants for the component atoms in the CPA medium and their concentration averaged values are shown. The decrease in the exchange coupling constant with decreasing volume per atom is in qualitative agreement with the experimentally observed decrease of T_C with increasing pressure for binary Invar alloys, such as Fe-Ni and Fe-Pt [see panel (b) of Fig. 54 of the review article by Wassermann[5]]. Note that the CPA ignores all effects related to fluctuations in the near-neighbor environment and yields essentially a mean-field result. It is thus unable to produce a change from the ferromagnetic to the antiferromagnetic interaction. The CPA invokes the effect of the average environment generated by all the component atoms and therefore, is unable to produce antiferromagnetic exchange, requiring very specific arrangement of near neighbors. Note also that the CPA is valid only as long as the magnetic properties of the component atoms are not too dissimilar. This makes the results for large lattice parameters in Fig. 13 unreliable.

IV. CONCLUSION

We have examined in detail the electronic structure, and cohesive, thermal, and magnetic properties of some disordered ternary Invar alloys. The results for these ternary alloys show remarkable similarity with the binary alloys with regard to the general Invar behavior. Ground-state properties of these Invar alloys show anomalies near the ferromagnetic to para(non)magnetic transitions, as observed in binary systems. The calculation of thermal-expansion coefficients, magnetic moments, and hyperfine fields are in qualitative agreement with the experimental trend. The transition from the ferromagnetic to the nonmagnetic state is shown to be accompanied by a sharp change in the charge density at the nuclei, which is a result of a major change in the electronic charge distribution at the transition. The disappearance of the local magnetic moment accompanies a transfer of charge from *d* to *s* states, causing a rapid increase in the charge density at the nuclear sites. This has been observed in ^{57}Fe Mössbauer shift experiments in the Fe-Ni system.[33] The results for the exchange coupling parameters, though overestimated in our CPA calculation, reproduce the correct trend with regard to variation with lattice parameter and composition. A detailed study of exchange interactions going beyond mean-field approximations is in progress.

ACKNOWLEDGMENTS

S.K.B. would like to thank Denis Rancourt and Ken Lagarec for discussions related to Invar alloys. The authors would also like to gratefully acknowledge numerous helpful discussions with Vaclav Drchal and Josef Kudrnovský on the LMTO-CPA method. This work was supported by a grant from the Natural Sciences and Engineering Research Council of Canada.

*Email address: bsanyal@newton.physics.brocku.ca
†Email address: bose@newton.physics.brocku.ca

[1] Ch. E Guillaume, C. R. Hebd. Seances Acad. Sci. **125**, 235 (1897).
[2] R. J. Weiss, Proc. Phys. Soc. London **82**, 281 (1963).
[3] M. Shiga, in *Materials Science and Technology*, edited by K. H. J. Buschow (VCH Verlagsgesellschaft mbH, Weinheim, 1994), Vol. 3B, p. 163.
[4] E. F. Wassermann, J. Magn. Magn. Mater. **100**, 346 (1991).
[5] E. F. Wassermann, in *Ferromagnetic Materials*, edited by K. H. J. Buschow and E. P. Wolfarth (Elsevier Science, Amsterdam, 1990), Vol. 5, p. 314.
[6] M. Podgórny, Phys. Rev. B **43**, 11 300 (1991); **46**, 6293 (1992).
[7] (a) O. K. Andersen, O. Jepsen, and M. Sob, in *Electronic Structure and its Applications*, edited by M. Youssouff, Lecture Notes in Physics Vol. 283 (Springer, Berlin, 1987), pp. 1-57; (b) O. K. Andersen, O. Jepsen, and D. Glötzel, in *Highlights of Condensed Matter Theory*, edited by F. Bassani, F. Fumi, and M. P. Tosi (North-Holland, Amsterdam, 1985), pp. 59-176.
[8] P. Entel, E. Hoffmann, P. Mohn, K. Schwarz, and V. L. Moruzzi, Phys. Rev. B **47**, 8706 (1993).
[9] I. A. Abrikosov, O. Eriksson, P. Söderlind, H. L. Skriver, and B. Johansson, Phys. Rev. B **51**, 1058 (1995).
[10] M. Schröter, H. Ebert, H. Akai, P. Entel, E. Hoffmann, and G. G. Reddy, Phys. Rev. B **52**, 188 (1995).
[11] E. G. Moroni and T. Jarlborg, Physica B **161**, 115 (1989).
[12] R. Hayn and V. Drchal, Phys. Rev. B **58**, 4341 (1998).
[13] H. Akai and P. H. Dederichs, Phys. Rev. B **47**, 8739 (1993); see also J. Staunton, B. L. Gyorffy, A. J. Pindor, G. M. Stocks, and H. Winter, J. Phys. F: Met. Phys. **15**, 1387 (1985); A. J. Pindor, J. Staunton, G. M. Stocks, and H. Winter, *ibid.* **13**, 979 (1983).
[14] W. E. Evenson, J. R. Schrieffer, and S. Q. Wang, J. Appl. Phys.

41, 1199 (1970); M. Cyrot, Phys. Rev. Lett. **25**, 871 (1970); D. G. Pettifor, J. Magn. Magn. Mater. **15-18**, 847 (1980).
[15] Y. Wang, G. M. Stocks, D. M. C. Nicholson, W. A. Shelton, V. P. Antropov, and B. N. Harmon, J. Appl. Phys. **81**, 3873 (1997).
[16] M. van Schilfgaarde, I. A. Abrikosov, and B. Johansson, Nature (London) **400**, 48 (1999).
[17] R. F. Sabiryanov, S. K. Bose, and O. N. Mryasov, Phys. Rev. B **51**, 8958 (1995).
[18] J. Kudrnovský and V. Drchal, Phys. Rev. B **41**, 7515 (1990).
[19] U. von Barth and L. Hedin, J. Phys. C **5**, 1629 (1972).
[20] V. L. Moruzzi, J. F. Janak, and K. Schwarz, Phys. Rev. B **37**, 790 (1988).
[21] C. Kittel, *Introduction to Solid State Physics*, 7th ed. (Wiley, New York, 1996), p. 126, Table 1.
[22] N. W. Ashcroft and N. D. Mermin, *Solid State Physics* (Saunders College, Philadelphia, Holt-Saunders International Edition, 1976), Chap. 25.
[23] G. T. Furukawa, T. B. Douglas, and N. Pearlman, in *American Institute of Physics Handbook* (McGraw-Hill, New York, 1957), Sec. 4e.
[24] R. A. MacDonald and W. M. MacDonald, Phys. Rev. B **24**, 1715 (1981).
[25] A. I. Liechtenstein, M. I. Katsnelson, and V. A. Gubanov, J. Phys. F: Met. Phys. **14**, L125 (1984); Solid State Commun. **54**, 327 (1985).
[26] A. I. Liechtenstein, M. I. Katsnelson, V. P. Antropov, and V. A. Gubanov, J. Magn. Magn. Mater. **67**, 65 (1987).
[27] A. R. Macintosh and O. K. Andersen, in *Electrons at the Fermi Surface*, edited by M. Springford (Cambridge University Press, London, 1980), p. 149.
[28] P. Lloyd and P. V. Smith, Adv. Phys. **21**, 69 (1972).
[29] I. Turek, J. Magn. Magn. Mater. **98**, 119 (1991).
[30] W. B. Pearson, *Handbook of Lattice Spacing and Structures of Metals and Alloys* (Pergamon, London, 1958), p. 640.
[31] Y. Kong, F. S. Li, M. Kaack, J. Pelzl, P. Stauche, and H. Bach, J. Phys.: Condens. Matter **12**, 2079 (2000).
[32] G. Hausch and H. Warlimont, Z. Metallkd. **63**, 547 (1972).
[33] K. Lagarec and D. Rancourt (private communication).
[34] F. Ono, M. Asano, R. Tanaka, and S. Endo, J. Magn. Magn. Mater. **90-91**, 757 (1990).
[35] J. Staunton, B. L. Gyorffy, A. J. Pindor, G. M. Stocks, and H. Winter, J. Magn. Magn. Mater. **45**, 15 (1984).
[36] D. G. Rancourt and M.-Z. Dang, Phys. Rev. B **54**, 12 225 (1996).
[37] M. Dubé, P. R. L. Heron, and D. G. Rancourt, J. Magn. Magn. Mater. **147**, 122 (1995).
[38] M.-Z. Dang, M. Dubé, and D. G. Rancourt, J. Magn. Magn. Mater. **147**, 133 (1995).